doi.org/10.36721/PJPS.2026.39.11.328.1

Jolkinolide B induces apoptosis and G1 arrest in A549 cells via JAK2/STAT3 inhibition

Jia Sun, Cili Jifu, Yanli Qiu, Linxia Lu, Zhenyu Xu, Zilin He and Jingtao Wang*
College of Basic Medicine, Jiamusi University, Jiamusi 154007, People's Republic of China

Abstract: **Background**: Lung cancer is the most common pulmonary malignancy. WHO data show that its incidence and mortality are rising globally, severely threatening public health. **Objectives**: This study aims to investigate the regulatory effect of Jolkinolide B (JB) on lung cancer A549 cells and to preliminarily explore the potential molecular mechanisms underlying its anti-lung cancer effects. **Methods**: In this study, A549 lung adenocarcinoma cells were used to investigate the anti-lung cancer effects of JB. CCK-8 and colony formation assays were performed to evaluate cell proliferation. Molecular docking and molecular dynamics simulation were applied to verify the binding between JB and JAK2, while Western blot was used to detect the expression of JAK2/STAT3 pathway-related proteins. Flow cytometry, immunofluorescence and Western blot were employed to explore the regulatory roles of JB in cell apoptosis and cycle. In addition, a nude mouse xenograft model was established and HE staining and immunohistochemistry were used to verify the *in-vivo* efficacy of JB. All data were statistically analyzed using GraphPad Prism and SPSS. **Results**: The results demonstrated that JB inhibited A549 cell proliferation in a dose-dependent manner with an IC_{50} of 39.34 μM at 24 h. JB bound stably to JAK2 (PDB: 7RN6) with a binding free energy of −8.33 kcal/mol and suppressed the JAK2/STAT3 pathway. JB significantly promoted apoptosis and induced G1-phase arrest via regulating P21, Cyclin D1, BAX, Caspase 3, PARP1 and Bcl-2. *In-vivo*, JB reduced tumor growth in a dose-dependent manner, induced tumor cell necrosis and downregulated p-JAK2 and p-STAT3 expression. **Conclusion**: Jolkinolide B can significantly inhibit the proliferation of human lung adenocarcinoma A549 cells. Its mechanism of action is closely related to inducing cell cycle arrest and promoting cell apoptosis. The above effects may be partially achieved by inhibiting the JAK2/STAT3 pathway. In animal experiments, JB also significantly inhibits the growth of lung cancer transplanted tumors.

Keywords: Apoptosis; Cell cycle; *Euphorbia fischeriana*; JAK2/STAT3; Jolkinolide B; Lung cancer

Submitted on 22-11-2025 – Revised on 08-03-2026 – Accepted on 14-04-2026

INTRODUCTION

Lung cancer has become an extremely serious health issue worldwide, contributing significantly to worldwide morbidity and mortality. Among all cancers, lung cancer has the highest incidence rate (about 12.4%) and mortality rate (about 18.7%) and is generally associated with a poorer prognosis; the five-year survival rate remains below 20% in most countries (Allemani *et al*., 2018; Bray *et al.*, 2024). Each year, more than 2 million new cases are diagnosed, leading to nearly 1.8 million deaths (Siegel *et al*., 2022). Historically, treatment strategies have been guided by histological classification, with chemotherapy serving as the cornerstone (Xu *et al*., 2025). Despite continuous improvements in diagnostic and therapeutic methods, survival outcomes for lung cancer patients remain unsatisfactory. Therefore, there is a critical need to develop novel treatment strategies and discover new effective drugs, including natural herbal medicines.

In recent years, research on the therapeutic effects and mechanisms of action of Chinese herbal medicines and their active ingredients (monomers) on various diseases, including lung cancer, has received extensive attention (Ma *et al*., 2024). JB is a diterpene compound monomer isolated and extracted from *Euphorbia fischeriana*. Multiple studies have demonstrated that it has strong biological activity against various diseases (Jian *et al*., 2018; Wang *et al*., 2022; Zhang *et al*., 2022). However, the exact mechanism by which JB combats lung cancer is not yet fully understood. JAK2/STAT3 pathway plays a significant role in tumorigenesis and tumor progression in various types of cancers (Lai *et al*., 2024; Huang *et al*., 2022; Liu *et al*., 2023). Constitutive active mutations of JAK2 were found in the irregular proliferation of some myeloid cells and leukemia (Wu *et al*., 2019). Studies have reported that JAK2/STAT3 pathway can serve as a key regulatory factor for activating CRC angiogenesis (Li *et al*., 2025). More and more evidence indicate that there is a certain connection between the dysregulation of JAKs/STATs and tumors (Miao *et al*., 2025; Bian *et al*., 2025; Liu *et al*., 2025).

Based on the above theory, this research investigated whether JB affects the occurrence and development of lung cancer, as well as the underlying mechanism of this effect, with the aim of identifying more effective treatment targets for lung cancer.

**Corresponding author:* e-mail: wjingtao@jmsu.edu.cn

MATERIALS AND METHODS

Experimental equipment, reagents and antibodies

In this study, the following instruments were used, for example: laser scanning confocal microscope (ZEISS, LSM910), Multifunctional microplate reader (Spark), ultra centrifuge (Nippon Hitachi, CP70MX), CO_2 incubator (Thermo Fisher Scientific, 3111), ultra cold storage freezer (Thermo, 994), Ventilated mouse cage (Monkey King, HH-A-4II), automatic tissue hydroextractor (Leica, RM2016), Vertical electrophoresis instrument (BIO-Rad, PROTEAN II), ultra microtome (Leica, UC7), flow cytometer (BD, BDFACSCALLBUR) and other large-scale precision equipment. JB was bought from TRC in Canada (item number: P468400). The acquisition of Cell Counting Kit-8 was supported by Meren Biotechnology Company. Dimethyl sulfoxide (DMSO) was purchased from Damao Chemical Reagent Factory (Tianjin, China). The membrane-associated protein V-FITC/PI kit was purchased from Kejun Biotechnology Co., Ltd. (Nanjing, China). The procurement of BALB/c nude mice was completed through Liaoning Changsheng Biotechnology Co, Ltd (Benxi, China) and these mice were approximately 4-5 weeks. The antibodies used in this study were as follows: Caspase 3 (Proteintech, 25128-1-AP), PARP1 (Proteintech, 13371-1-AP), BAX (Proteintech, 50599-2-Ig), Bcl-2 (Proteintech, 26593-1-AP), p-JAK2 (ABmart, T56570F), JAK2 (ZENBIO, R24775), STAT3 (ZENBIO, 251611), p-STAT3 (ABmart, TC52210S), Cyclin D1 (Proteintech, 269-1-AP), P21 (Proteintech, 27296-1-AP), GAPDH (Proteintech, 10494-1-AP) and anti-rabbit IgG (Cell Signaling Technology). The dilution ratios were 1:2000, 1:2000, 1:5000, 1:2000, 1:500, 1:500, 1:500, 1:500, 1:2000, 1:2000, 1:5000, 1:10000, respectively.

Cell culture

The A549 human lung adenocarcinoma cells were purchased from Procell System (item number CL-0016) and were accompanied by STR identification. These cells need to be cultured in a constant-temperature and humidity incubator at 37°C with 5% carbon dioxide. The culture medium contains 10% fetal bovine serum (Liang *et al*., 2019).

Cell counting Kit-8 assays

Following digestion, A549 cells were diluted and seeded into 96-well plates for culture (Liang *et al*., 2019). Approximately 10,000 cells were counted in each well and 100 microliters of culture medium were added to each well. Three duplicate Wells were set up for each experimental group. Then it was incubated in a CO_2 incubator for 24 h. After adhesion, JB of the specified concentration and 10 microliters of CCK-8 solution were added to each well. Incubate for 0.5- 2 h depending on the situation. Finally, the absorbance was measured at 450 nm using an enzyme detector, with the data read once every hour.

Colony formation assays

A549 cells were seeded into six-well plates at a density of approximately 100 cells per well. The cell-seeded six-well plates were transferred to an incubator and incubated for 24 h until full cell adhesion was obtained. Once the experimental criteria were fulfilled, JB was administered to the cells and the culture medium was renewed every 2-3 days. Subsequently, the cells were rinsed with PBS, fixed with 4% formaldehyde solution and finally stained with a certain proportion of crystal violet solution (G1064, Solbo Biotechnology, China) for 10 min (Zhang *et al*., 2023). Imaging was performed using ImageJ software and quantitative analysis of clones was conducted.

Immunofluorescence

Approximately 1×10^5 A549 cells were inoculated into 6 cm culture dishes. After 24 h of incubation, the cells were fixed with 4% paraformaldehyde. Subsequently, the slides were incubated in PBS containing 1% bovine serum albumin (BSA) for 30 min. Primary antibodies against BAX and Bcl-2 were applied at a dilution of 1:200. The slides were incubated overnight at 4°C with the two primary antibodies, rinsed three to five times with PBS and further incubated with secondary antibodies (1:500) for 1h. Thereafter, the slides were mounted with DAPI-containing anti-fade medium (P0131-25 mL, Bio-Trend) and stored at 4°C. Finally, cellular images were acquired under a fluorescence microscope (Liang *et al*., 2019).

Flow cytometry (Apoptosis detection)

A549 cells were treated with JB for 24 h. Following treatment, the culture medium was gently aspirated into centrifuge tubes. The adherent cells were digested using EDTA-free trypsin and the detached cell suspension was pooled with the collected medium. The mixed cell suspension was centrifuged at 1200 rpm for 5 min; the supernatant was subsequently discarded and the cell pellet was preserved. The cell pellet was softly resuspended in 100μL of apoptosis detection binding buffer. In accordance with the kit manufacturer's protocols, 10μL Annexin V-FITC staining solution and 5μL PI staining solution were sequentially added. The staining reagents were gently blended and samples were incubated in the dark at room temperature. After incubation, 400μL of pre-cooled binding buffer was supplemented to each flow tube to reach a final volume of 500μL. The prepared samples were gently homogenized and immediately subjected to flow cytometric detection (Liang *et al*., 2019).

Flow cytometry (Cell cycle analysis)

The A549 cells were seeded in 6-well plates at a density of approximately 5×10^4 cells per well, followed by treatment with JB for 24 h. After treatment, cells were harvested and fixed in pre-cooled 70% ethanol overnight at -20 °C. After fixation, cells were centrifuged and washed twice with cold PBS to remove ethanol. The cells were then incubated with RNase A (100μg/mL) for 30

min at 37°C to eliminate RNA interference. Subsequently, the cells were stained with propidium iodide (PI, 50 μg/mL) in the dark for 15 min at room temperature. Flow cytometric analysis was performed using a BD Calibur flow cytometer. Cell cycle distribution was analyzed using Mod Fit LT software, in which doublet discrimination (FSC-H vs FSC-A or PI-W vs PI-A gating) was applied to exclude cell clumps, doublets and aggregated cells, ensuring accurate quantification of DNA content in single cells (Zhang *et al*., 2023).

Western blot

Collected cells were lysed and homogenized using RIPA lysis buffer (SIBO, China) supplemented with protease inhibitors. Following lysis, the protein concentration of each sample was quantified via the BCA assay and the loading volume of each sample was calculated accordingly. Extracted protein samples were mixed with loading buffer and boiled in a water bath for 5 min to achieve complete protein denaturation. Subsequently, 5–10 μL of each protein sample was loaded onto 12% SDS-PAGE gels for electrophoresis, after which the separated proteins were electrotransferred onto PVDF membranes. The membranes were then blocked with defatted milk at room temperature. After blocking, the membranes were incubated with primary antibodies overnight, followed by incubation with corresponding secondary antibodies at room temperature for 1 h. Protein bands were visualized using an ECL chemiluminescence kit and captured with a gel imaging system. The relative expression level of target proteins was quantified by calculating the gray value ratio of target proteins to the corresponding internal reference proteins (Liang *et al*., 2019).

In-vivo tumor xenograft model

This study adhered to the ARRIVE guidelines for animal research reports. According to the animal ethics guidelines of Qiqihar Medical University, BALB/c nude mice (healthy nude mice, 4-5 weeks old, randomly divided into male and female groups, weighing 15-20 g; Liaoning Changsheng) were used. This school has an independent experimental animal center that can carry out the entire research process, including breeding and raising experimental animals, establishing disease animal models and conducting *in-vivo* pharmacological animal experiments in a single step. The mice were randomly divided into 4 groups (4 mice in each group), totaling 16 mice (Liang *et al*., 2019). The sample size was determined based on previous studies and preliminary experiments to ensure adequate statistical power. Subcutaneous xenografts were established via flank inoculation of 5×10^6 tumor cells. When the tumor volume reached 100 mm^3, the mice were randomly divided into four experimental groups. Every 1-2 days, 200 μL of blank solvent or JB at low (4 mg/kg), medium (6 mg/kg) and high (8 mg/kg) doses was administered by intraperitoneal injection. Tumor dimensions and body weight were measured biweekly; volume = (length × width²)/2. Mice were euthanized and tumors were collected for analysis.

Hematoxylin-eosin staining

After JB administration, mice were sacrificed to harvest tumor tissues, which were fixed in 4% paraformaldehyde for ≥24 h. Fixed tissues underwent gradient ethanol dehydration, xylene clearing and paraffin embedding. Serial 3 μm paraffin sections were floated, mounted on adhesive slides and baked. For HE staining, sections were dewaxed and rehydrated. Hematoxylin-stained slides were washed for bluing, differentiated in hydrochloric acid–ethanol, rinsed for clear nuclear staining and then counterstained with eosin. Slides were rapidly dehydrated, cleared, mounted with neutral balsam and air-dried. Tumor pathological morphology was visualized under light microscopy and representative images were acquired for statistical analysis (Brázdil *et al*., 2022).

Immunohistochemistry (IHC)

Tissue sections were dewaxed in xylene and rehydrated through graded ethanol. Antigen retrieval was performed in citrate buffer (pH 6.0) using a high-pressure cooker. After cooling, sections were incubated with 3% hydrogen peroxide for 10 min at 25 °C to inhibit endogenous peroxidase activity. Non-specific binding was blocked with normal serum for 30 min at room temperature. The sections were incubated with primary antibodies overnight at 4 °C, followed by incubation with HRP-conjugated secondary antibodies for 1 h at room temperature. Immunoreactivity was visualized using a DAB chromogenic reaction, which was terminated by rinsing with distilled water. Sections were counterstained with hematoxylin, dehydrated, cleared and mounted. Finally, protein expression was observed under a light microscope and quantitatively analyzed based on staining intensity and positive area (Brázdil *et al*., 2022).

Molecular docking simulation

The three-dimensional crystal structure of JAK2 (PDB: 7RN6) was obtained from the Protein Data Bank. Crystallographic water, small molecules, metal ions and redundant polypeptide chains were removed using PyMOL 2.5 to generate the pure receptor protein, which was saved in PDB format. The small-molecule ligand was optimized geometrically and converted to PDBQT format via Open Babel 2.4.1. Hydrogen atoms, Gasteiger charges and rotatable bonds were added and defined for the receptor and ligand using AutoDock Tools 1.5.6. The docking box was centered at the active site with coordinates X=18.903, Y=-13.354, Z=-12.518, box dimensions of 108 A×148 A×150 A and grid spacing of 0.464 A. Molecular docking was performed using AutoDock Vina 1.2.3 with the Lamarckian Genetic Algorithm (LGA) for conformational search and 10 independent runs were set to ensure sampling sufficiency. The optimal conformation was selected based on the

lowest binding energy (kcal/mol). PyMOL 2.5 was applied for structural optimization, hydrogen bond identification, hydrophobic interaction analysis and visualization to illustrate the interactions between the JB ligand and key residues of the target protein (Bisht *et al*., 2024).

Molecular dynamics (MD)

Gromacs 2022.3 software was used for molecular dynamics simulation. For small molecule preprocessing, AmberTools 22 was used to add the GAFF force field to small molecules, while Gaussian 16W was used to hydrogenate small molecules and calculate RESP potential. Potential data will be added to the topology file of the molecular dynamics system. The simulation conditions were carried out at a static temperature of 300K and atmospheric pressure (1 Bar). Amber99sb-ildn was used as the force field; water molecules were used as the solvent (Tip3p water model) and the total charge of the simulation system was neutralized by adding an appropriate number of Na+ions. The simulation system was minimized using the steepest descent method and then equilibrated in the isothermal-isovolumic ensemble (NVT) and isothermal-isobaric ensemble (NPT) for 100000 steps, respectively, with a coupling constant of 0.1 ps and a duration of 100 ps. Finally, the free molecular dynamics simulation was performed. The process consisted of 50000000 steps; the step length was 2 fs and the total duration was 100 ns. After the simulation was completed, the built-in tool of the software was used to analyze the trajectory and the root-mean-square deviation (RMSD) and root-mean-square fluctuation (RMSF) (Bisht *et al*., 2024).

Statistical analysis

Statistical analysis was conducted using SPSS software and bar charts were also drawn using GraphPad. The inter-group comparisons were performed using analysis of variance and the *P* values were corrected using the LSD method. The results were presented in the form of mean ± standard deviation. Statistical significance was defined as a *P* value less than 0.05. The test data conform to the statistical methods.

RESULTS

Effects of JB on the viability and proliferation of A549 cells in-vitro

In the first step of the experiment, the CCK-8 method was used to determine cell viability after exposure to JB at concentrations of 0 μM, 5 μM, 10 μM, 20 μM, 40 μM and 80 μM for 24 hours. The results indicated that cell viability decreased with increasing drug concentration, with a median lethal concentration (IC50) of 39.34 μM (Fig. 1A). Consequently, JB concentrations of 0 μM, 10 μM, 20 μM and 30 μM were selected for subsequent experiments.

The colony formation assay is a classic method for evaluating cell proliferation ability. This method was used to assess cell proliferation and the results are as follows: compared with the control group, the number of A549 cell clones in the JB-treated group decreased significantly, the clone volume became smaller and this decrease occurred in a concentration-dependent manner (Fig. 1B). The inhibitory effect of JB on A549 cell proliferation was most significant at a concentration of 30 μM. Combined with the above CCK-8 experimental results, these data initially confirm that JB has an inhibitory effect on the viability and proliferation of A549 cells, allowing for subsequent experimental studies.

Effects of JB on the JAK2/STAT3 signaling pathway of A549 cells in-vitro

The JAK2/STAT3 pathway serves as a crucial regulatory mechanism in tumor progression. To verify the regulatory effect of JB on the JAK2/STAT3 pathway in A549 cells, molecular docking analysis was performed to explore the potential interaction between JB and the core JAK2 protein (PDB: 7RN6). The interaction modes of key amino acid residues and the binding status within the active site are presented in the corresponding figure. The calculated binding free energy was -8.33 kcal/mol, suggesting a strong binding affinity (Fig. 2A).

Molecular dynamics simulations verified the high binding stability between JB and JAK2. The RMSD values of the complex and protein backbone were 0.28 nm and 0.23 nm, respectively and the ligand RMSD was as low as 0.04 nm, indicating stable binding without obvious dissociation. RMSF analysis revealed reduced flexibility of JAK2 residues, especially around the binding pocket, suggesting that JB stabilizes the protein conformation via noncovalent interactions. These results demonstrate strong and stable binding of JB to JAK2 at the dynamic level, supporting its potential as a bioactive modulator (Fig. 2B).

To verify the reliability of the molecular docking results, experimental verification was subsequently performed. The expression levels of JAK2, p-JAK2, STAT3 and p-STAT3 were detected by Western blot following JB treatment. The results showed that JB inhibited the phosphorylation of JAK2 and STAT3 and this inhibitory effect was dose-dependent (Fig. 2C).

Effects of JB on apoptosis of A549 cells in-vitro

To explore whether the changes in cell viability induced by JB treatment are associated with apoptosis, flow cytometry and Western blotting analyses were performed. The flow cytometry results demonstrated that the total apoptosis rate of A549 cells in the control group was 9.5% (Fig. 3A). After JB treatment, the total apoptosis rates increased to 17.37%, 20.96% and 25.36%, respectively, with the high-dose group showing a more significant increase. Results of the WB analysis experiment proved that JB significantly upregulated the expression levels of BAX, Caspase 3 and PARP 1 and simultaneously downregulated the expression of Bcl-2 (Fig. 3B). These findings highlight the pro-apoptotic effect of JB.

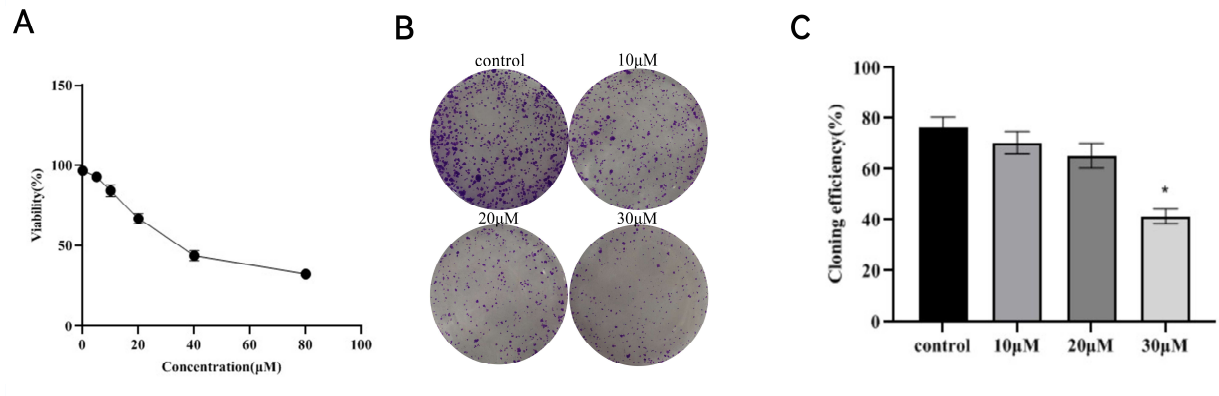

Fig. 1: Effects of JB on the viability and proliferation of A549 cells
(A) CCK-8 to detect proliferative capacity of A549 cells; (B) Cloning assays to detect clone formation of A549 cells; (C) Data are presented as mean ± SD (n = 3). **P* < 0.05; ***P* < 0.01; ****P* < 0.001; *****P* < 0.0001, ns: no statistical difference vs control group.

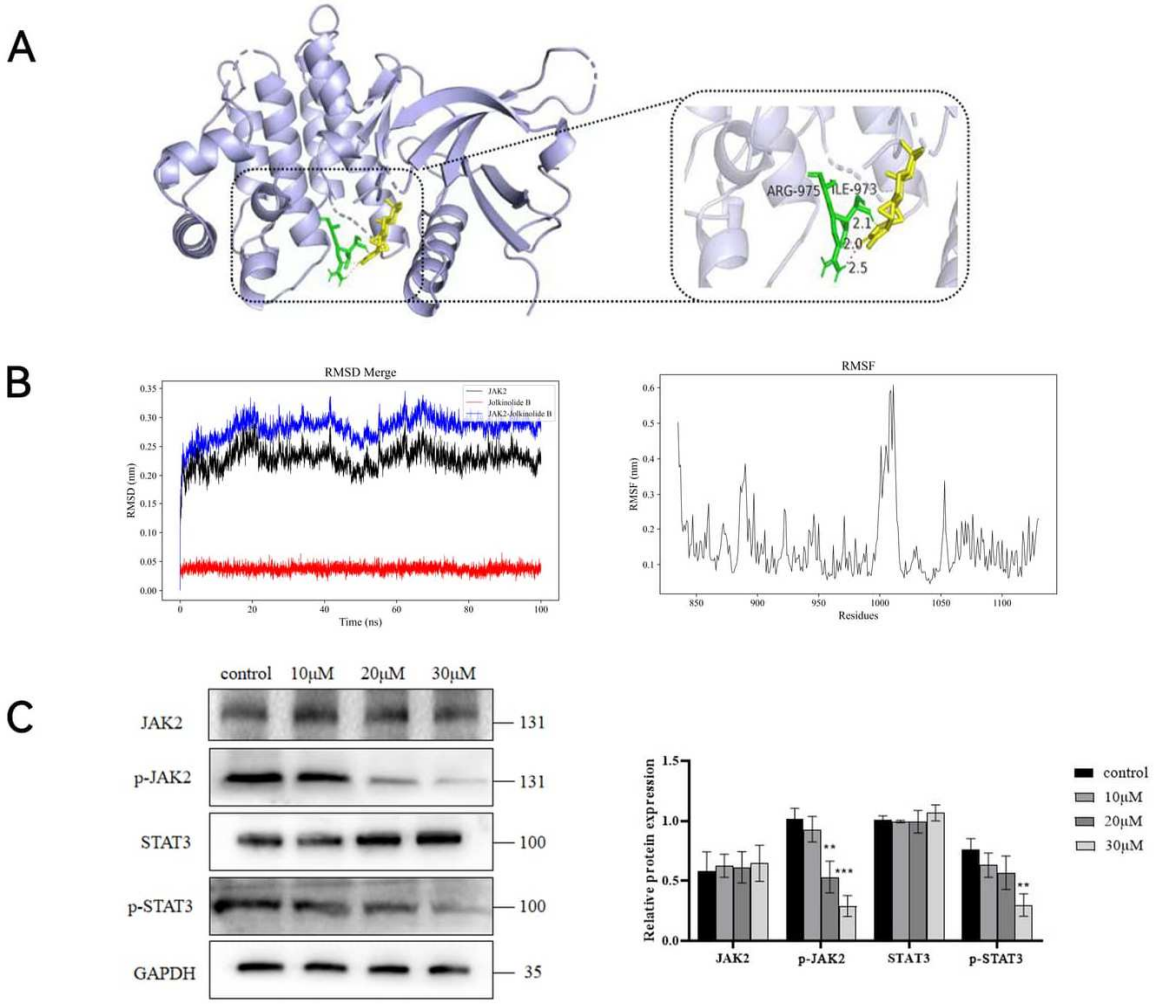

Fig. 2: Effects of JB on the JAK2/STAT3 pathway of A549 cells *in-vitro*
(A) Results of molecular docking validation for interactions between the core protein JAK2 and JB; (B) Molecular dynamics simulation verifies stability; (C) Western blot analysis of pathway markers JAK2, p-JAK2, STAT3 and p-STAT3. Data are presented as mean ± SD (n = 3). **P* < 0.05; ***P* < 0.01; ****P* < 0.001; *****P* < 0.0001, ns: no statistical difference vs control group.

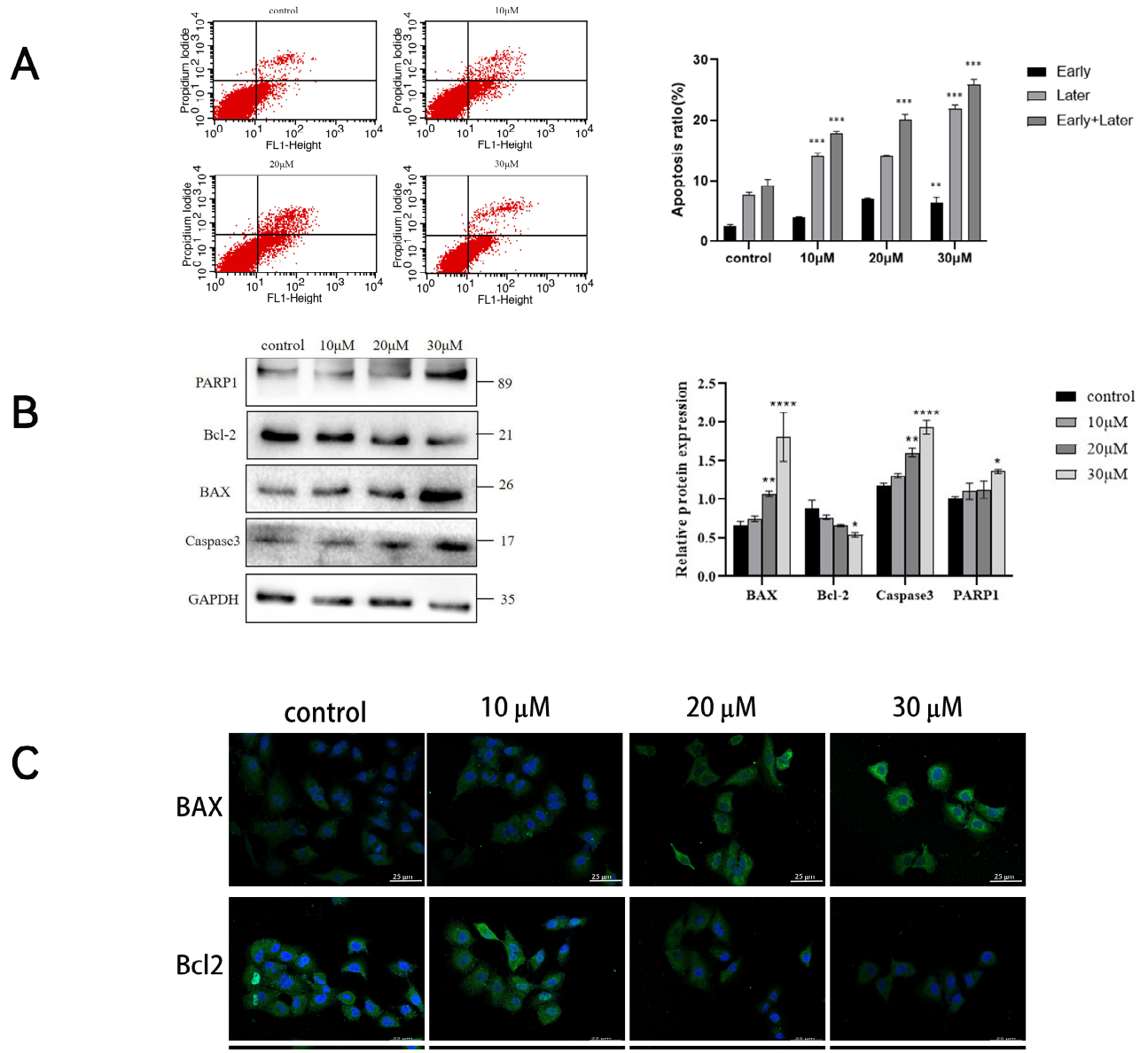

Fig. 3: Effects of JB on apoptosis of A549 cells *in-vitro*
(A) Detection of apoptosis in A549 cells by flow cytometry. Record and analyze the values of early apoptosis, late apoptosis, and total apoptosis; (B) Western blot analysis of apoptotic markers: BAX, PARP 1, Caspase 3 and Bcl-2; (C) Immunofluorescence staining showing the expression of apoptosis-related proteins BAX and Bcl-2, ×400. Data are presented as mean ± SD (n = 3). **P* < 0.05; ***P* < 0.01; ****P* < 0.001; *****P* < 0.0001, ns: no statistical difference vs control group.

Immunofluorescence analysis was further conducted to detect BAX and Bcl-2 expression. The results revealed distinct expression patterns of the two proteins in lung cancer cells: under JB stimulation, BAX expression increased in a dose-dependent manner, accompanied by significantly enhanced green fluorescence intensity. In contrast, Bcl-2 expression was dose-dependently reduced, with a marked decrease in green fluorescence intensity (Fig. 3C). Collectively, these data confirm that JB induces apoptosis in A549 cells, thereby inhibiting their growth.

Effects of JB on cell cycle of A549 cells in-vitro

To explore the specific correlation between cell cycle arrest and the inhibitory effect of JB on A549 cell growth, cell cycle analysis was subsequently performed by flow cytometry and the expression of P21 protein was detected via Western blot. Flow cytometry results revealed that the proportion of A549 cells arrested in the G0/G1 phase gradually increased with increasing drug concentration. The proportions of the four groups were determined as 62.17%, 70.09%, 76.04% and 87.01%, respectively.

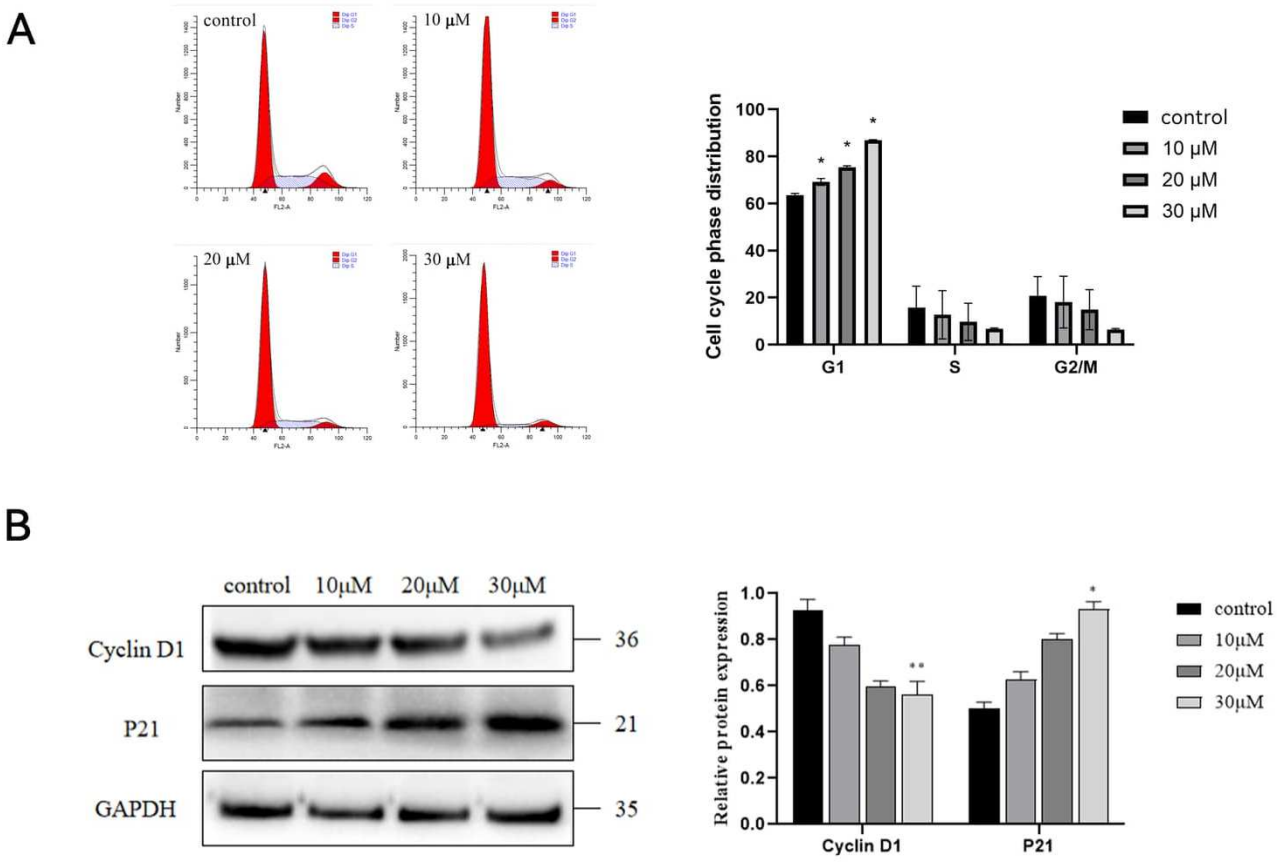

Fig. 4: Effects of JB on cell cycle of A549 cells *in-vitro*
(A) The cell cycle distribution of A549 cells was detected by flow cytometry, and the percentage of cell populations in the G1, S and G2 phases; (B) Western blot analysis of apoptotic markers: P21 and Cyclin D1.
Data are presented as mean ± SD (n = 3). **P* < 0.05; ***P* < 0.01; ****P* < 0.001; *****P* < 0.0001, ns: no statistical difference vs control group.

Meanwhile, the proportions of cells in S phase and G2/M phase showed a downward trend, but the reduction extent was not obvious and no significant difference was observed. Based on the above findings, it is confirmed that JB can induce specific G1 phase cell To explore the specific correlation between cell cycle arrest and the inhibitory effect of JB on A549 cell growth, cell cycle analysis was subsequently performed by flow cytometry and the expression of P21 protein was detected via Western blot. Flow cytometry results revealed that the proportion of A549 cells arrested in the G0/G1 phase gradually increased with increasing drug concentration. The proportions of the four groups were determined as 62.17%, 70.09%, 76.04% and 87.01%, respectively. Meanwhile, the proportions of cells in S phase and G2/M phase showed a downward trend, but the reduction extent was not obvious and no significant difference was observed. Based on the above findings, it is confirmed that JB can induce specific G1 phase cell cycle arrest in A549 cells (Fig. 4A). Western blot analysis demonstrated that JB treatment significantly up-regulated the expression level of P21 protein and this promoting effect was dose-dependent. In addition, the expression level of Cyclin D1 protein was gradually down-regulated with the increase in JB concentration (Fig. 4B). cycle arrest in A549 cells (Fig. 4A). The results of Western blot analysis demonstrated that the expression level of P21 protein was significantly up-regulated by JB treatment and this promoting effect was dose-dependent. In addition, the expression level of Cyclin D1 protein was gradually down-regulated with the increase in JB concentration (Fig. 4B).

Effects of JB on lung cancer cells in-vivo

To enrich the experimental design, the antitumor activity of JB was further verified *in-vivo*. First, it is necessary to establish a subcutaneous transplantation model of mouse lung cancer cells and administer the drug according to the experimental design. The results of *in-vivo* experiments on animals showed that JB significantly inhibited tumor growth in mice. Compared with the control group, the size and weight of the tumors in the treatment group decreased as the drug concentration increased (Fig. 5A). Compared with the control group, the inhibition rate of the low-dose JB group was 25.19% ± 0.98%, that of the medium-dose group was 44.33% ± 1.88% and that of the high-dose group was 56.78% ± 5.33%.

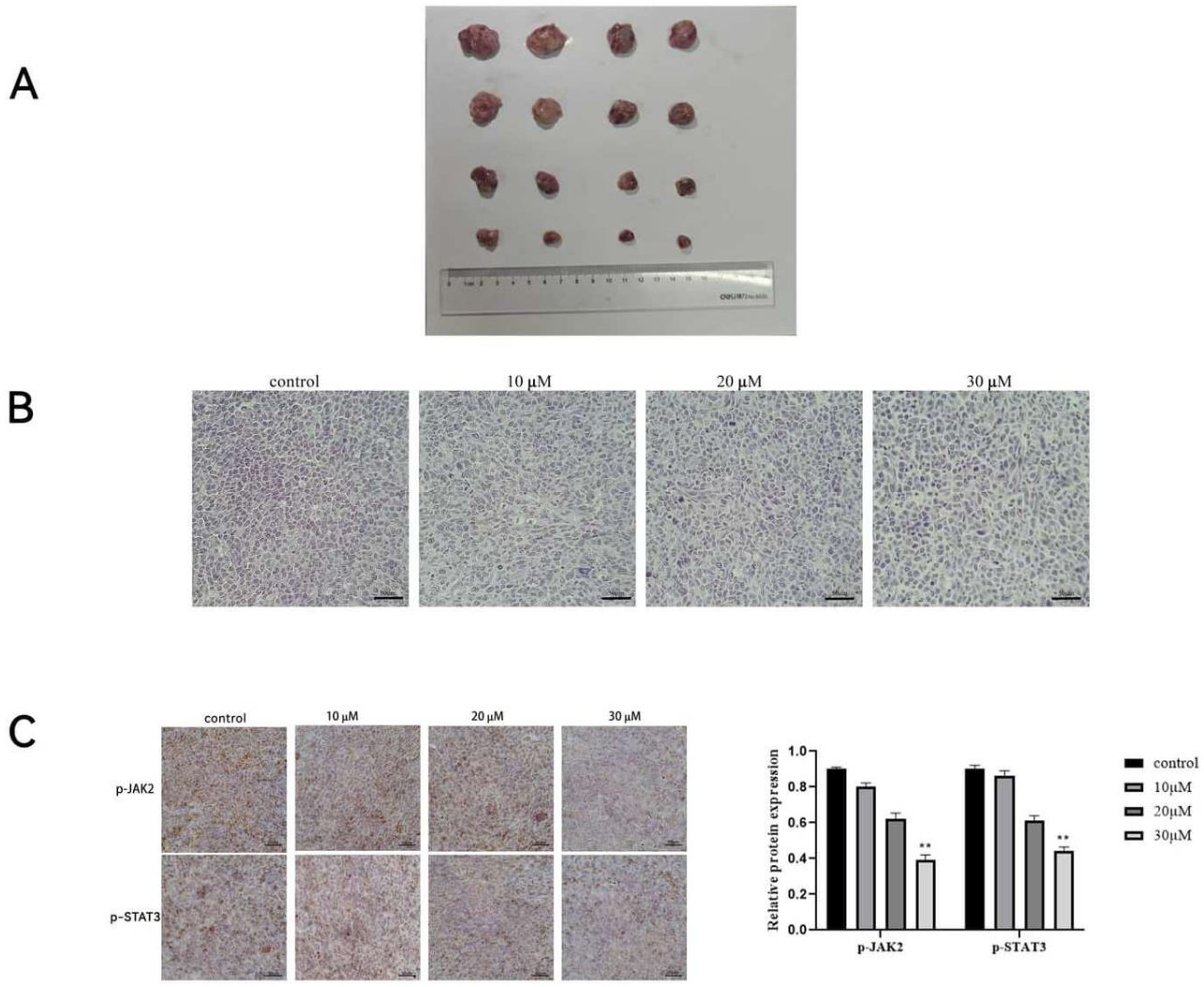

Fig. 5: Effects of JB on lung cancer cells *in-vivo*

(A) The tumor tissues were arranged from top to bottom in the order of the control group, low-dose group, medium-dose group and high-dose group. The volumes of the mouse tumor tissues were observed; (B) Hematoxylin-eosin (HE) staining analysis showed the histological structure of tumor tissues, from left to right; they are the control group, the low-dose group, the medium-dose group and the high-dose group. HE, ×200; (C) Immunohistochemical findings of lung cancer, from top to bottom: p-JAK2 and p-STAT3 proteins; from left to right, they are the control group, the low-dose group, the medium-dose group and the high-dose group, IHC, ×200. Data are presented as mean ± SD (n = 4). *$P < 0.05$; **$P < 0.01$; ***$P < 0.001$; ****$P < 0.0001$, ns: no statistical difference vs control group.

The results of the *in-vivo* experiments were consistent with those of the *in-vitro* cell experiments, indicating that JB has an anti-tumor effect. This may be achieved by inhibiting cell proliferation and promoting cell apoptosis, reducing the number of tumor cells and thereby suppressing tumor development. The results of HE staining indicated that the tumor cells in the model group were densely arranged, with no infiltration of immune cells, no necrosis and the cell nuclei were large and deeply stained. In the low-dose JB group, partial nuclear shrinkage was observed. In the high-dose group, tumor cells exhibited irregular arrangement, disrupted cell membranes, nuclear shrinkage and prominent vacuolation accompanied by necrosis (Fig. 5B).

Subsequently, immunohistochemistry (IHC) was performed to confirm that JB affects xenograft tumor tissues via the JAK2/STAT3 signaling pathway. Compared with the control group, JB treatment significantly down-regulated the expression levels of p-JAK2 and p-STAT3 in tumor tissues (Fig. 5C). In summary, *in-vivo* experiments demonstrated that JB exerts anti-lung cancer effects via targeting the JAK2/STAT3 pathway, which is consistent with the findings obtained from the preceding *in-vitro* experiments.

DISCUSSION

Lung cancer is one of the most prevalent malignant tumors worldwide. Projections indicate that the global annual

incidence of lung cancer will rise to 3.8 million cases by 2050, with an annual mortality of approximately 3.2 million (Sung *et al*., 2020). Currently, clinical therapeutic strategies for lung cancer mainly include chemotherapy, surgical resection and targeted therapy. However, only one-third of patients are diagnosed with surgically resectable stage I-IIIa tumors in clinical practice. Despite continuous advancements in surgical techniques and the optimization of perioperative management protocols, the 5-year survival rate of such patients remains only 38% to 60% (Detterbeck *et al*., 2021), which is considerably lower than that of most common malignant tumors. The main cause of this poor outcome is the presence of micrometastatic foci that are difficult to eliminate with perioperative chemoradiotherapy. In recent years, the emergence of novel therapeutic strategies, such as targeted therapy and immune checkpoint inhibitors, has revolutionized the clinical diagnosis and treatment paradigm for advanced non-small cell lung cancer (NSCLC) and has effectively improved patient prognosis (Reck *et al*., 2021). Nevertheless, the overall prognosis of lung cancer remains unfavorable, with a 5-year overall survival rate of only 19.3% (Siegel *et al*., 2022). These findings underscore the urgent need to explore new treatment strategies and develop highly effective anti-lung cancer drugs.

Terpenoids are promising natural anti-tumor substances that have been proven to exert chemotherapeutic and chemopreventive effects on a variety of tumors. Compared with traditional chemotherapeutic drugs, natural terpenoid-based agents offer better efficacy and fewer adverse reactions (Li *et al*., 2022). Terpenoids can be divided into diterpenoids, triterpenoids and other subclasses, among which diterpenoids with isoprene or isopentane skeletons are the core active components of *Euphorbia fischeriana* (Li *et al*., 2022). JB is one of the most bioactive diterpenoids isolated from *Euphorbia fischeriana*. Multiple studies have confirmed that JB exerts anti-tumor activity against a variety of solid tumors and leukemia: JB induces apoptosis and cell cycle arrest in gastric cancer cells *in-vitro* and inhibits gastric tumor growth *in-vivo*; it also induces apoptosis in MCF-7 breast cancer cells through the PI3K/Akt/mTOR pathway (Jian *et al*., 2020; Wang *et al*., 2022) and suppresses the metastatic potential of MDA-MB-231 breast cancer cells. In addition, structural analogs of JB have been shown to target the thioredoxin and glutathione systems, inducing reactive oxygen species (ROS)-mediated apoptosis in bladder cancer cells. In this study, cytological assays including CCK-8 and colony formation experiments were used to investigate the effect of JB on the viability of A549 lung cancer cells. The results confirmed that the inhibitory effect of JB on the survival rate of A549 cells was dose-dependent: the proliferative capacity of A549 cells decreased significantly as JB concentration increased, which was consistent with previous findings.

The JAK/STAT pathway is pivotal in regulating fundamental biological processes, including cell proliferation, differentiation, cell cycle progression, metastasis and apoptosis (Chen *et al*., 2022). The Janus kinase (JAK) family consists of four members: JAK1, JAK2, JAK3 and TYK2. These kinases activate signal transducers and activators of transcription (STATs) through phosphorylation, thereby mediating cytokine signal transduction. Once phosphorylated, STAT proteins dimerize and translocate to the nucleus, where they modulate immune responses and the transcription of inflammation-related genes (Hu *et al*., 2021).

Among these transcription factors, STAT3 serves as a core regulator of cytokine-mediated signaling (Jin *et al*., 2022). Its activation is primarily achieved through JAK2-mediated phosphorylation at the tyrosine 705 (Y705) residue (Rawlings *et al*., 2020). As a non-receptor tyrosine kinase, JAK2 functions by binding to cytokine receptors: cytokines such as interleukin-6 (IL-6) and erythropoietin (EPO) bind to their respective receptors, triggering JAK2 activation. Activated JAK2 then phosphorylates the intracellular domain of the receptor, creating docking sites for downstream signaling molecules such as STAT3. Under physiological conditions, STAT3 is phosphorylated by activated JAK2, translocates from the cytoplasm to the nucleus, binds to DNA and regulates the transcription of target genes involved in cell growth, survival and immune responses (Mengie *et al*., 2022). In this study, molecular docking revealed a strong binding affinity between JB and the JAK2 protein and molecular dynamics simulations further confirmed the high stability of this interaction. Based on the above findings, this study further explored the mechanism of the JAK2/STAT3 signaling pathway. Both *in-vitro* and *in-vivo* experimental results demonstrated that JB significantly downregulated the expression levels of phosphorylated JAK2 (p-JAK2) and phosphorylated STAT3 (p-STAT3). Collectively, these results indicate that JB may exert anti-non-small cell lung cancer activity by suppressing the activation of the JAK2/STAT3 pathway.

Apoptosis and cell cycle dysregulation are two core characteristics of tumor occurrence and progression and they coordinately control the malignant proliferation of tumor cells. Apoptosis is a highly conserved and precisely regulated mode of programmed cell death during biological evolution. It plays a pivotal role in maintaining the homeostasis of the internal environment, eliminating damaged and abnormally proliferating cells and participating in embryonic development, immune regulation, as well as the occurrence and progression of various diseases (Bertheloot *et al*., 2021). Dysregulation of apoptosis is a typical feature of tumors. Under physiological conditions, cell apoptosis exerts a tumor-suppressive effect by eliminating precancerous cells; however, when the balance between cell division and death is disrupted, tumor cells escape apoptotic signals, leading to unlimited proliferation and promoting tumor progression (Wong *et al*., 2021; Fulda *et al*., 2022). Therefore, cell apoptosis is not only an important regulatory link in tumorigenesis and development, but also a core target for tumor treatment and inducing tumor cell apoptosis is an effective strategy for clinical cancer treatment. Research has

shown that a variety of stimuli, including viral infection, hyperthermia, hypoxia and oxidative stress, can induce cell apoptosis. Stress signals elicited by chemoradiotherapy act on the mitochondrial outer membrane, triggering the release of cytochrome c from the mitochondrial intermembrane space into the cytoplasm. This process facilitates apoptosome formation and activates Caspase-3/7, ultimately resulting in tumor cell apoptosis (Eskandari *et al*., 2022).

Mechanistically, apoptosis is mediated by specific cysteine proteases (caspases), which initiate the intrinsic and extrinsic apoptotic cascades. The intrinsic pathway is triggered by mitochondrial injury, which drives apoptosome assembly and subsequent activation of caspase-9. As the central executioner of apoptosis, caspase-3 is cleaved and activated by upstream caspase-8 or caspase-9. Activated caspase-3 further targets and degrades multiple key cellular proteins, inducing the typical morphological features that serve as hallmark indicators of apoptotic cell death. (Bhat *et al*., 2023; Zhou *et al*., 2020). This study found that JB markedly induces apoptotic cell death in NSCLC cells in a concentration-dependent fashion. Flow cytometry results showed that JB at concentrations of 10 μM, 20 μM and 30 μM could promote the apoptosis of NSCLC cells and the apoptotic rate increased as the drug concentration rose. The results of Western blot and immunofluorescence experiments further confirmed that changes in apoptosis-related protein expression were consistent with the apoptotic trend, indicating that JB exerts a tumor-suppressive effect by inducing apoptosis in A549 lung cancer cells.

Cell cycles serve as another vital therapeutic target for inhibiting the abnormal proliferation of tumor cells. Cell cycle arrest can effectively block tumor cells from entering the proliferative stage, thereby suppressing their unlimited proliferation and invasion. The cell cycle consists of four proliferative phases, namely G1, S, G2 and M, as well as a quiescent G0 phase. Stimulated by mitogenic factors and growth factors, cells enter the G1 phase, rapidly synthesize substances required for DNA replication, expand organelles and complete their own growth; after reaching a certain volume, they enter the S phase to initiate DNA replication and then enter the G2 phase to check the completion of DNA replication and synthesize substances related to mitosis. During the M phase, cells initiate mitosis, assemble the mitotic spindle and separate sister chromatids. This process ensures that daughter cells receive identical sets of chromosomes before division is completed. After finishing division, cells return to the G1 phase, forming the repeating G1-S-G2-M cell cycle (Gupta *et al*., 2022; Tyson *et al*., 2022). When cells are stimulated by external factors or receive division termination signals, they can enter the G0 quiescent phase to stop division, which is a reversible process: cells can re-enter the cell cycle after removing the stimulating factors (Pack *et al*., 2019), while continuous stimulation will cause cells to exit the cell cycle and even undergo apoptosis (Gousias *et al*., 2022).

The G1/S transition is a key regulatory node in cell cycle progression, where cells decide to continue proliferation, undergo apoptosis or enter a quiescent state (Zheng *et al*., 2019). Studies have confirmed that P21 can directly bind to the cyclin-cyclin-dependent kinase (cyclin-CDK) complex and inhibit its phosphorylation of downstream target proteins (Shamloo *et al*., 2019). To further explore the molecular mechanism by which JB regulates cell cycle progression, flow cytometry was used to detect cell cycle distribution in A549 cells and the expression levels of the cell cycle-regulatory proteins P21 and Cyclin D1 were determined. The results revealed that treatment with different concentrations of JB markedly upregulated P21 expression while significantly downregulating Cyclin D1. These findings suggest that JB modulates the expression of cell cycle-associated proteins, thereby inducing G1-phase cell cycle arrest in lung cancer cells.

In conclusion, this study confirmed that JB exerts a significant anti-lung cancer effect and its core mechanisms are inducing apoptosis of lung cancer cells and arresting cells in the G1 phase. Meanwhile, JB can regulate the JAK2/STAT3 pathway and significantly inhibit the expression of p-JAK2 and p-STAT3 in both lung cancer cells and xenograft models, which is an important pathway for it to mediate anti-tumor activity.

Research limitations

The effects of JB were only validated in A549 cells and subcutaneous xenograft models, with other lung cancer subtypes not included in the present study. Furthermore, the off-target effects of JB remain unclear. In future investigations, a comparison between JB and clinically approved JAK inhibitors (e.g., ruxolitinib) will be conducted and the underlying drug resistance mechanisms will be further explored.

CONCLUSION

In conclusion, the compound JB exhibits a significant inhibitory effect on the proliferation of A549 cells. Such suppression is achieved through the induction of cell cycle arrest and the promotion of cell apoptosis. These biological activities may be partially attributed to the inhibition of the JAK2/STAT3 pathway by JB. *In-vivo* animal models have further verified that JB markedly restrains the growth of lung cancer tumors. These findings not only highlight the therapeutic potential of *Euphorbia fischeriana* (the source plant of JB) in lung cancer treatment, particularly lung adenocarcinoma, but also advance the understanding of the molecular mechanisms underlying JB action. This provides valuable insights for the development of novel anticancer therapies with optimized specificity and safety. Nevertheless, the present study still possesses certain limitations. Although the

JAK2/STAT3 pathway has been identified as a key regulatory axis, the precise molecular mechanism of JB and its potential off-target effects remain to be further elucidated. Moreover, clinical trials are required to evaluate the efficacy of JB as a promising therapeutic candidate for lung cancer patients.

Acknowledgments
None.

Author's contributions
Jia Sun: Writing-review and editing, writing-original draft, resources, methodology, investigation, formal analysis, data curation and conceptualization; Yanli Qiu: Writing-review and editing, writing-original draft and conceptualization; Cili Jifu: Data curation, conceptualization; Zilin He: Formal analysis, data curation and conceptualization; Zhenyu Xu: Methodology, investigation and resources, analysis, data curation and conceptualization; Linxia Lu: Writing-review and editing, writing-original draft, data visualization, supervision and resources; Jingtao Wang: Project administration, methodology, investigation, funding acquisition and data curation.

Funding
This study was supported by the Key Research and Development Program of Heilongjiang Province (22024ZX12009).

Data availability statement
The data that support the findings of this study are available from the corresponding author upon reasonable request.

Ethical approval
This study was approved by the Ethics Committee of the Qiqihaer Medical University (QMU-AECC-2025-251). This clinical study complies with relevant ethical regulations (Vijayananthan and Nawawi, 2008). This study was approved by the Ethics Committee for exemption from informed consent and all data were anonymized. This study was performed in adherence with the ARRIVE guidelines. See supplementary file for the ARRIVE checklist.

Conflict of interest
The authors declare no conflict of interest.

Supplementary data
https://pjps.pk/uploads/2026/08/SUP1787212724.pdf

REFERENCES

Allemani C, Matsuda T, Di Carlo V, Harewood R, Matz M, Niksic M, Bonaventure A, Valkov M, Johnson CJ, Estève J, Ogunbiyi OJ, Azevedo E Silva G, Chen WQ, Eser S, Engholm G, Stiller CA, Monnereau A, Woods RR, Visser O and Lim GH (2018). Global surveillance of trends in cancer survival 2000-14 (CONCORD-3): analysis of individual records for 37 513 025 patients diagnosed with one of 18 cancers from 322 population-based registries in 71 countries. *Lancet*., **391**(10125): 1023-1075.

Brazdil T, Gallo M, Nenutil R, Kubanda A, Toufar M and Holub P (2022). Automated annotations of epithelial cells and stroma in hematoxylin-eosin-stained whole-slide images using cytokeratin re-staining. *J Pathol Clin Res*., **8**(2): 129-142.

Bisht A, Tewari D, Kumar S and Chandra S (2024). Network pharmacology, molecular docking and molecular dynamics simulation to elucidate the mechanism of anti-aging action of Tinospora cordifolia. *Mol Divers*., **28**(3): 1743-1763.

Bian X, Chen Y, Zhang C, Huang S, Fu X, Yang B, Lu S, Zhao W, Pan Y and Zhao S (2025). NR4A3high mast cells promote ovarian cancer metastasis by reprogramming tumor-associated macrophages via JAK2/STAT6 signaling. *Transl Oncol*., **60**: 102494.

Bray F, Laversanne M, Sung H, Ferlay J, Siegel RL, Soerjomataram I and Jemal A (2024). Global cancer statistics 2022: GLOBOCAN estimates of incidence and mortality worldwide for 36 cancers in 185 countries. *CA Cancer J Clin*., **74**(3): 229-263.

Bertheloot D, Latz E and Franklin BS (2021). Necroptosis, pyroptosis and apoptosis: An intricate game of cell death. *Cell Mol Immunol*., **18**(5): 1106-1121.

Bhat AA, Thapa R, Afzal O, Agrawal N, Almalki WH, Kazmi I, Alzarea SI, Altamimi ASA, Prasher P, Singh SK, Dua K and Gupta G (2023). The pyroptotic role of caspase-3/GSDME signalling pathway among various cancer: A Review. *Int J Biol Macromol*., **242**(Pt 2): 124832.

Chen Y, Li X, Zhang L (2022). JAK/STAT signaling pathway in cancer: From pathogenesis to targeted therapy. *Signal Transduct Target Ther*., **7**(1): 369.

Detterbeck FC, Chansky K and Goldstraw P (2021). The IASLC lung cancer staging project: Background, objectives and methodological considerations. *J Thorac Oncol*., **16**(1): 20-31.

Eskandari E and Eaves CJ (2022). Paradoxical roles of caspase 3 in regulating cell survival, proliferation and tumorigenesis. *J Cell Biol*., **221**(6): e202201159.

Fulda S and Vucic D (2022). Targeting cell death pathways in cancer therapy: Recent progress and future perspectives. *Curr Opin Cell Biol*., **76**: 102-110.

Gousias K, Theocharous T and Simon M (2022). Mechanisms of cell cycle arrest and apoptosis in glioblastoma. *Biomedicines*., **10**(3): 564.

Gupta VK and Chaudhuri O (2022). Mechanical regulation of cell-cycle progression and division. *Trends Cell Bio*., **32**(9): 773-785.

Hu X, li J, Fu M, Zhao X and Wang W (2021). The JAK/STAT signaling pathway: From bench to clinic. *Signal Transduct Target Ther*., **6**: 402.

Huang B, Lang X and Li X (2022). The role of IL-6/JAK2/STAT3 signaling pathway in cancers. *Front Oncol*., **12**: 1023177.

Jian B,Zhang H and Liu J (2018). Structural diversity and biological activities of diterpenoids derived from *Euphorbia fischeriana Steud*. *Molecules*., **18**(4): 935.

Jian B, Zhang H and Liu J (2020). Diterpenoids from *Euphorbia fischeriana* and their cytotoxic activity against human cancer cell lines. *Molecules*., **25**(18): 4215.

Jin Y, Kang Y, Wang M, Wu B, Su B, Yin H, Tang Y, Li Q, Wei W, Mei Q, Hu G, Lukacs-Kornek V, Li J, Wu K, Yuan X and Wang W (2022). Targeting polarized phenotype of microglia via IL6/JAK2/STAT3 signaling to reduce NSCLC brain metastasis. *Signal Transduct TargetTher*., **7**(1): 52.

Lai JQ, Zhao LL, Hong C, Zou QM, Su JX, Li SJ, Zhou XF, Li ZS, Deng B, Cao J and Qi Q (2024). Baicalein triggers ferroptosis in colorectal cancer cells via blocking the JAK2/STAT3/GPX4 axis. *Acta Pharmacol Sin*., **45**(8): 1715-1726.

Liu Y, Xu Q, Deng F, Zheng Z, Luo J, Wang P, Zhou J, Lu X, Zhang L, Chen Z, Zhang Q, Chen Q and Zuo D (2023). HERC2 promotes inflammation-driven cancer stemness and immune evasion in hepatocellular carcinoma by activating STAT3 pathway. *J Exp Clin Cancer Res*., **42**(1): 38.

Li P, Liu G, Zhang W, Li T and Yang X (2025). Prkci activates Jak2/Stat3 signaling to promote tumor angiogenesis: Short Name: Prkci in tumor angiogenesis. *Neoplasia*., **68**: 101219.

Liang L, Hui K, Hu C, Wen Y, Yang S, Zhu P, Wang L, Xia Y, Qiao Y, Sun W, Fei J, Chen T, Zhao F, Yang B and Jiang X (2019). Autophagy inhibition potentiates the anti-angiogenic property of multikinase inhibitor anlotinib through JAK2/STAT3/VEGFA signaling in non-small cell lung cancer cells. *J Exp Clin Cancer Res*., **38**(1): 71.

Liu H, Liu T, Zeng J and Fang Q (2025). Silymarin induces multiple myeloma cell apoptosis by inhibiting the JAK2/STAT3 signaling pathway. *Oncol Lett*., **30**(3): 426.

Li Y, Zhang H and Wang Y (2022). Phytochemical profiling and biological activities of *Euphorbia fischeriana Steud*: A review. *J Ethnopharmacol*., **296**: 115347.

Mengie Ayele T, Tilahun Muche Z, Behaile Teklemariam A, Bogale Kassie A and Chekol Abebe E (2022). Role of JAK2/STAT3 signaling pathway in the tumorigenesis, chemotherapy resistance and treatment of solid tumors: A systemic review. *J Inflamm Res*., **15**: 1349-1364.

Ma C, Gao L, Song K, Gu B, Wang B, Pu W and Chen H (2024). Jolkinolide B inhibits gastric cancer growth by targeting the PANoptosis molecular switch caspase-8. *J Cancer*., **15**(18): 6038-6051.

Miao Y, Yang S, Zhang F, Li J and Zhang Y (2025). Discovery and biological evaluation of a novel and highly potent JAK2 inhibitor for the treatment of triple negative breast cancer. *J Enzyme Inhib Med Chem*., **40**(1): 2488127.

Pack LR, Daigh LH and Meyer T (2019). Putting the brakes on the cell cycle: Mechanisms of cellular growth arrest. *Curr Opin Cell Biol*., **60**: 106-113.

Reck M, Rodríguez-Abreu D and Robinson AG (2021). Pembrolizumab plus chemotherapy for metastatic non-small-cell lung cancer. *N Engl J Med*., **384**(19): 1803-1813.

Rawlings JS and Harrison DA (2020). JAK-STAT signaling: Recent advances and new complexities. *Immunity*., **53**(5): 973-987.

Sung H, Ferlay J and Siegel RL (2021). Global cancer statistics 2020: GLOBOCAN estimates of incidence and mortality worldwide for 36 cancers in 185 countries. *CA Cancer J Clin*., **71**(3): 209-249.

Siegel RL, Miller KD, Fuchs HE and Jemal A (2022). Cancer statistics, 2022. *CA Cancer J Clin*., **72**(1): 7-33.

Shamloo B and Usluer S (2019). p21 in cancer research. *Cancers (Basel)*., **11**(8): 1178.

Tyson JJ and Novak B (2022). Time-keeping and decision-making in the cell cycle. *Interface Focus*., **12**(4): 20210075.

Wang Y, Shen SY, Liu L, Zhang XD, Liu DY and Liu N (2022). Jolkinolide B inhibits proliferation or migration and promotes apoptosis of MCF-7 or BT-474 breast cancer cells by downregulating the PI3K-Akt pathway. *J Ethnopharmacol*., **282**: 114581.

Wu QY, Ma MM, Zhang S, Cao J, Yan ZL, Chen C, Li ZY, Zeng LY, Wang XY, Li F and Xu KL (2019). Disruption of R867 and Y613 interaction plays key roles in JAK2 R867Q mutation caused acute leukemia. *Int J Biol Macromol*., **36**: 209-219.

Wong RS, Gulati R and Burger AM (2021). Apoptosis in cancer: From pathogenesis to targeted therapy. *J Exp Clin Cancer Res*., **40**(1): 219.

Xu Y, Zhang K, Ye Z, Huang Z, Chen R, Zhang Y, Zhang H and Kou L (2025). Nanomedicine initiates ferroptosis for enhanced lung cancer therapy. *Drug Deliv*., **32**(1): 2527752.

Zhou M, Liu X and Li Z (2020). Caspase 3 regulates cancer cell migration and invasion via cleaving cytoskeletal proteins. *Oncogene*., **39**(45): 6789-6802.

Zheng L, Zhao Z, Rong L, Xue L and Song Y (2019). RASSF6-TRIM16 axis promotes cell proliferation, migration and invasion in esophageal squamous cell carcinoma. *J Genet Genomics*., **46**(10): 477-488.

Zhang X, Zheng X, Ying X, Xie W, Yin Y and Wang X (2023). CEBPG suppresses ferroptosis through transcriptional control of SLC7A11 in ovarian cancer. *J Transl Med*., **21**(1):334.

Zhang H, Qian J, Jin M, Fan L, Fan S and Pan H (2022). Jolkinolide B induces cell cycle arre stand apoptosis in MKN45 gastriccancer cells and inhibits xenograft tumor growth *in-vivo*. *Biosci Rep*., **42**(6): BSR20220341.